Proceedings of the 7th International Symposium on Cavitation
CAV2009 – Paper No. ##
August 17-22, 2009, Ann Arbor, Michigan, USA

Slip effects in vortical structure behind cavitating propeller wake

Bu-Geun Paik, Kyung-Youl Kim and Ki-Sup Kim
Maritime & Ocean Engineering Research Institute, KORDI
Daejeon, Korea

ABSTRACT

The cavitating propeller wake is investigated in detail using PIV and shadow graph techniques to figure out the trace ability of bubble type of tracers, naturally generated by the decrease of the static pressure in a cavitation tunnel. Experiments are conducted in the conditions of the cavitating propeller wake containing strong vortices. The flow behaviors of bubble tracers are compared with those of normal solid particles. The bubbles grown from the nuclei melted in the cavitation tunnel could not influence on the additional buoyancy, producing good trace ability in the uniform flow.

The comparison between bubbles and solids shows some discrepancies in the area around the tip vortex core of cavitating propeller wake. The slip velocity, indicating the difference of moving velocities between bubble and solid, induces rather high difference in the vorticity values of it. The results of comparison in terms of vorticity values showed good agreement in the region of mild Re_S (Reynolds number based on the slip velocity), however, disagreement at high Re_S over 1000. The large slip velocity and high Re_S provided a velocity difference, especially in the high velocity gradient region. The slipstream region gives a range of $15 < Re_S < 75$; however, Re_S is about 1000 at a high velocity gradient region of a tip vortex. The fitted vorticity reduction rate would give a reference for the prediction in a real flow when bubble tracers are utilized in PIV measurements of a vortical flow. The vorticity reduction rates are obtained according to the bubble size which is considered to affect the slip effect in the high velocity gradient region.

INTRODUCTION

The PIV technique as a field measurement, needs uniformly distributed tracers in the flow for the appropriate measurements since it can have the measurement range of a few m to a few m. In addition, the tracer has the size of from a few nm to a few mm with the variation of the experimental conditions and the size of measurement plane. As the size of tracer is getting larger, the light intensity scattered from the tracer within the laser light sheet is also getting higher and this can provide some merits to the PIV measurement. However, larger tracers may play a role of additional nuclei in the cavitation tunnel and affect the cavitation patterns to some degree. As a result, the PIV measurements can not be conducted together with the cavitation observation tests in a tunnel and lead to some harsh works to clean the whole cavitation tunnel after them. MOERI(Maritime and Ocean Engineering Research Institute)'s mid-size cavitation tunnel holds water of about 50 tons and the cleaning works to remove tracer particles were available after PIV measurements. Recently, MOERI has been constructing another cavitation tunnel, which will have large test section of 2.8 x 1.8 x 12.5 m^3 and contain about 2100 tons of water. In this new cavitation tunnel, the cleaning works are considered to be nearly impossible because they will require too much cost and time. Therefore, serious considerations would be necessary for the effective employment of the PIV measurements in the large cavitation tunnel as well as the mid-size one.

The typical experiments carried out in the MOERI's mid-size cavitation tunnel consists of the reproduction of the ship's hull wake, propeller performance tests, rudder cavitation observation [1] and so on. For the realization of the hull wake, the equipment called the wake screen made of several steel meshes is used to simulate the wake flows behind the bare hull. Since this wake screen has quite fine and dense meshes, many tiny bubbles can be generated additionally. Although the large cavitation tunnel does not need the wake screen but ship model, it would be meaningful to investigate the trace ability of the bubbles in the presence of the wake screen for the expansion of the PIV application. The tunnel pressure should be controlled to match the propeller operation condition and lots of bubbles occurred when it is decreased under the water vapor pressure.

Studies on the bubbly flow have been performed by many researchers. Brenn et al. [2] investigated the unsteady two-phase flow with small rising bubbles using PDA (phase Doppler anemometry). They reveal information about flow behaviors of two-phase system through relative (slip) velocities. The increase in drag on bubbles due to interaction between bubbles and turbulence was introduced numerically by Lane et al. [3]. Bubble size effect was investigated on the gravity-driven pumping by injecting gas in the pipe using four point fiber probe and LDA (laser Doppler anemometry) [4].

The PIV measurements for two-phase flow have been performed to obtain velocity fields in the bubbly flows. Lindken at al.[5] have done the studies to separate each velocity component of the liquid or the vapor in the bubbly flow. Although Jansen et al.[6] investigated the breaking wave containing bubbles using the fluorescent particles and

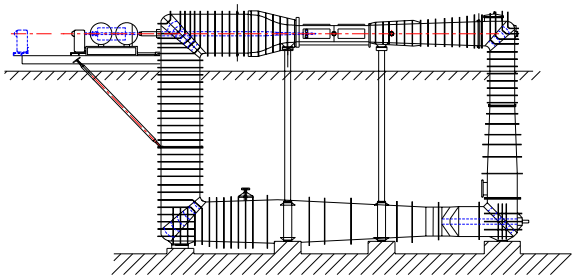

Figure 1: Schematic diagram of the cavitation tunnel

ultraviolet rays; they do not show good spatial resolution of velocity field. Govender et al.[7] showed insufficient explanation of the PIV technique itself though he tried to get some information on the two-phase flow. It is necessary to study the details about the light source because the intensity of the scattered light from the bubbles is small in the bubbly flow with low void fraction and small-size bubbles. Ryu et al.[8] have conducted successfully PIV measurements based on the silhouette technique considering the bubbles as the tracer to visualize the green water over the head deck of a ship.

In the present study, the propeller wake as a high velocity gradient flow was investigated with using bubbles generated naturally by the decrease of a tunnel pressure. Especially, velocity fields were extracted to confirm the PIV technique using bubble tracers in the propeller wake of high Reynolds number over 10^6. In addition, the reason why some discrepancies between two tracer cases occur was investigated in the viewpoint of the slip velocity and the bubble size. A reference data was also provided to correct vorticity values in the results of bubbly flow.

EXPERIMENTAL SET UP

The experiments have been conducted in the mid-size cavitation tunnel of MOERI. The rectangular test section has dimensions of $0.6^H \times 0.6^W \times 2.6^L$ m^3. The maximum flow speed is 12m/s, and the pressure can be varied from 0.1 to 2.0 Kg$_f$/cm^2. A schematic diagram of the tunnel is shown in Fig. 1. The two-frame PIV system consists of a dual-head Nd:YAG laser (200mJ per pulse), two CCD cameras, a synchronizer, and a frame grabber as shown in Fig. 2. The CCD cameras have a resolution of 1024 × 1024 pixels, and a thin laser light sheet was used to illuminate the center plane longitudinally and capture the pairs of particle images separated by short time intervals by using the frame-straddling method. Velocity fields were extracted using the PIV algorithm of a cross-correlation method based on the FFT. The field of view was 10 cm × 10 cm in the uniform flow and the measurements were conducted to observe the behaviors of tracers with the variation of experimental conditions as shown in Table 1. The tunnel flow speed was detected from the Pitot tube installed on the wall ahead of the test section.

In this study, the propeller wake was measured to find out the likelihood of bubbles as tracers in the 2-D PIV technique. The propeller model for the container ship model has 5 blades, the mean pitch ratio of 0.990 and the diameter of 250mm. The wake screen was arranged in front of the propeller model to consider the bare hull wake. The propeller revolution is determined by the identity condition of the thrust in the cavitation tunnel. The significant decrease in tunnel pressure for the sake of the generation of bubbles may result in the reduction of the thrust, mismatching the design condition of the propeller. Therefore, bubble generation has to be considered after finding appropriate revolution condition. The present study satisfied well the thrust identity.

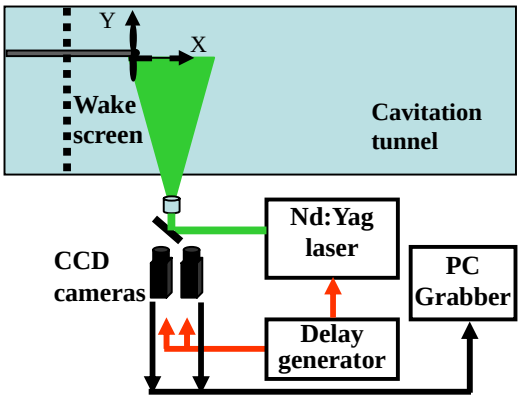

Figure 2: Schematic diagram of 2-D PIV experimental setup

The analysis of measurement uncertainties or precision errors was carried out for actual particle images whose flow field was known in advance. The quiescent flow was tested for the uncertainty evaluation of the present PIV system by following the procedure recommended by Raffel et al.[9] to estimate the measurement errors of PIV systems under the same condition as explained in the experimental apparatus and method. The standard errors encountered in measuring the displacement vector were calculated. To minimize the measurement uncertainties, 150 instantaneous velocity fields were ensemble averaged in the post-processing. As a result, the uncertainty levels measured by PIV system were 0.038% and 0.063% for the axial and radial velocity vectors, respectively. Instantaneous velocity fields were obtained for each measurement phase. They were ensemble-averaged to obtain the time-averaged in-plane velocity, vorticity, turbulence intensity and Reynolds shear stress in terms of tracers for PIV.

In addition, the bubble size was measured by using the shadowgraph technique with the images of bubbles as tracers. Although the shadowgraph technique may give rather less accurate sizing values than phase Doppler or global rainbow methods, we employed it because of the absence of other bubble sizing equipments. One strong light bulb was utilized to illuminate the bubbles at the side wall as shown in Fig. 3. The visualization system consisted of a high-speed camera (Photron, FASTCAM SA1.1), a Nikon 50mm lens (f # = 1.4), metal lamps (Photron, HVC-SL), an image processor, and a PC. The camera frame rate was 5000 fps (frames per second), since the flow speed was fixed in the propeller wake case. The spatial resolution and the size of the measurement plane were 1024 x 1024 pixels and 5.7 x 5.7 cm^2, respectively. The bubble size

was determined from the occupied pixels by a bubble, the measurement area and the spatial resolution of the camera.

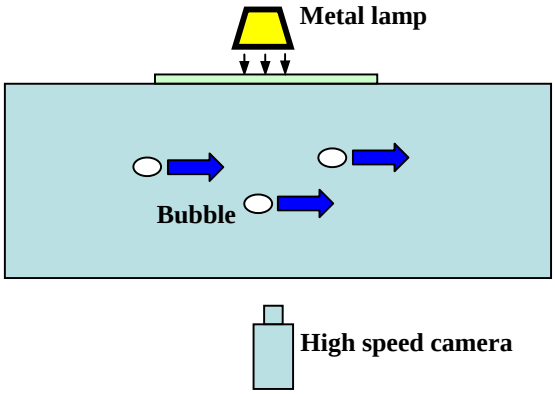

Figure 3: Sketch of the shadowgraph visualization set-up

RESULTS

The size of bubbles was measured at the condition of propeller operation. The experimental conditions were free stream speed of 7.01m/s, 25 propeller revolutions per second, and variable tunnel pressure from 1 atm.(atmospheric pressure) to 0.29 atm. Figure 4 shows the photo captured at the condition of 0.38 atm. as a typical example of shadow images. 300 photo images were investigated to obtain the bubble size distribution. The photo images have clear and blurred bubble images simultaneously according to the focal depth of the lens. The aperture number of lens was fixed to 1.4 to decrease the focal depth as much as possible. Using the threshold method the blurred bubbles were ruled out from the candidates of size measurements.

Figure 4: Photo image captured at 0.38 atm.

Actually, we have done the bubble size measurements in the uniform flow beforehand and those results are expressed in Table 1 together with the results of the propeller wake. The distinct differences between uniform flow and propeller wake were propeller operation and wake screen. The wake screen having many grids can provide smaller bubbles (than uniform flow) as well as high bubble concentration.

Table 1. Bubble size measured at uniform flow and propeller wake

Type	U_0(m/s)	P_t(atm.)	Size(mm)
Uniform flow	3	0.2	0.74 ± 0.24
	5	0.2	1.03 ± 0.13
	8	0.2	1.60 ± 0.11
Propeller wake	7	0.43	0.22 ± 0.11
		0.38	0.36 ± 0.19
		0.35	0.52 ± 0.26
		0.32	0.47 ± 0.14
		0.29	0.58 ± 0.15

Figure 5 and 6 show the photo image of bubbles and phase-averaged axial velocity distribution behind the propeller. The bubbles collected into tip vortices with strong vortex strength and low pressure values in their cores. Although they seem to look like the cavity tube of tip vortices, they are not actual continuous cavity tube. In addition, the patterns collected by bubbles were clearly different in each photo image and showed strong unsteadiness. Thus, we did not have any error induced by continuous cavity tube around the tip and trailing vortices in the PIV analysis.

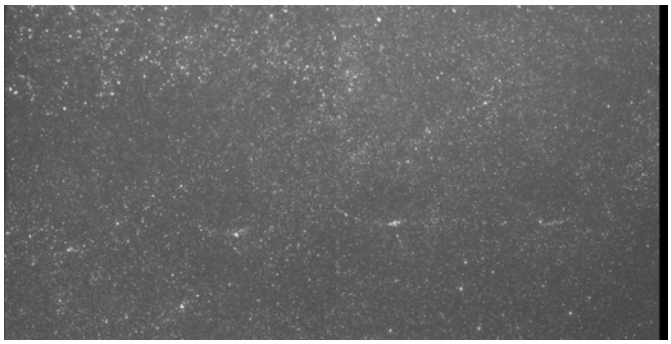

Figure 5: Photo image with bubble tracers at 0.29 atm.

The interrogation window size for PIV measurements was 50% overlapped 32 x 32 pixels in the propeller wake. The size of the measurement plane was 20 x 10 cm^2. The propeller wake has a quite complicated flow structure that consists of hub vortices, tip vortices and trailing vortices. The hub vortices were excluded in this study because the diffused reflection from them was too strong to capture the tracer images. The tip vortices are generated from the pressure difference between the suction and pressure sides at the blade tip region. The trailing edge of a blade produced the trailing vortices, which look like a curved layer connected to a tip vortex. At the atmospheric pressure, the aperture of the CCD camera was fully widened to capture the images of the tiny solid particles. On the other hand, the aperture was narrowed tightly so that it would not damage the CCD cells below the condition of 0.43 atm. because the light intensity scattered from the bubbles was very strong.

Figure 6 shows the contour plots of phase-averaged axial velocity at the rotation phase angle(ϕ) of 0° when the bubble tracers are put into the tunnel water. Here, the propeller axis locates along the line of Y/D = 0 and the propeller plane positioned at X/D = 0. The axial velocity component has large

values in the slipstream, which means that the region has high axial momentum inside the trajectories of tip vortices and relatively smaller values near the blade tip and the propeller axis. Along the tip region (-0.5 < Y/D < -0.4) of each blade, there are pairs of negative and positive iso-contours with the shape of a circle because of tip vortices. The velocity cores of Rankin type may give the information on vortex size from the characteristics of vortex. This tendency is very similar to the result from the solid particles. The result of the bubble tracers shows the contours location and shapes similar to that of solid particles. Although the magnitudes of axial velocity in the slipstream region are a little different between solid and bubble cases, the bubbles seem to show a trace ability as good as the solid tracers.

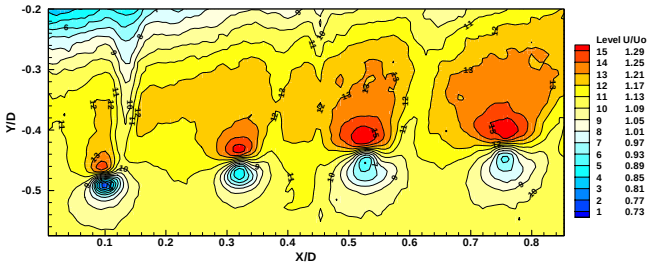

(a) 0.29 atm.

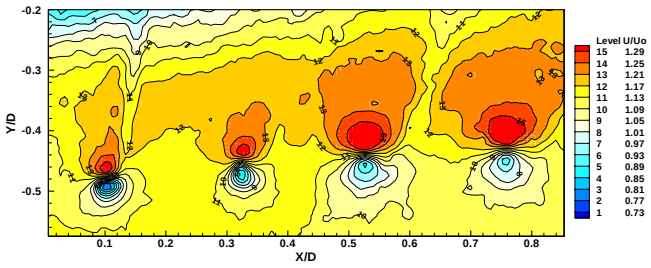

(b) 1 atm.

Figure 6: phase-averaged axial velocity contours at the same phase angle

The Z-directional vorticity(ω_Z) values of the trailing vortices in the bubble tracer case are similar to those in solid tracers, and the contours in the bubble case show a slightly broader distribution than those of solids as shown in Fig. 7. For the tip vortices, however, they became to have slightly deformed shape and smaller vorticity values in the bubble case because of the bubbles entrained into the tip vortex. Actually, bubble concentration around tip vortices is different from that of other region. In the tip vortex region the bubble concentration was about 184/1202 pixels and it reduced to 75/1202 pixels at the sandwiched region between tip vortices. The bubbles accumulated near vortex cores and resulted in the reduction of velocity magnitudes of bubbles, which is closely related to the decrease in vorticity value at the tip vortex region of the bubble case. However, the locations of the tip and trailing vortices are very similar in both tracer cases. These findings led us to learn that a flow visualization using bubble tracers can be carried out in terms of the spatial configuration of a complicated flow. For example, the variation of the blade pitch of a propeller changes the spatial spacing between the tip and trailing vortices in a wake flow. Although the PIV technique using bubble tracers can not measure the voriticity value accurately in a high velocity gradient region such as a vortex core, it would be helpful in diagnosing the parameters affecting the spatial evolution of the flows.

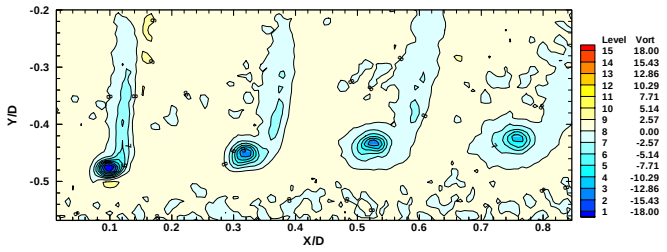

(a) 0.29 atm.

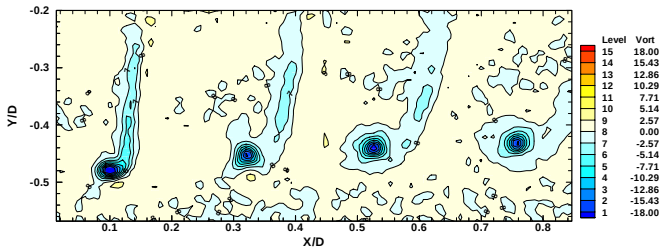

(b) 1 atm.

Figure 7: phase-averaged vorticity contours at the same phase angle

The maximum vorticity value of each tip vortex is decreasing as the wake moves downstream at 0.29 atm., which is compared to the result of 1 atm. with constant vorticity value at every tip vortex core. The core of a tip vortex has the strongest vorticity value in the propeller wake except the hub vortices. The vorticity value at the cores decreased gradually up to 2nd tip vortex in the case of 1 atm. as shown in Fig. 8. And thereafter, the decrease of the vorticity value was stopped. Other cases except 1 atm. show similar reduction rates of vorticity to that of 1 atm. from the first tip vortex to the second tip vortex, however, they have rather smaller reduction rate from the second tip vortex.

The linear fitted line had an equation of P = 19.5Q – 24.0 at 1 atm. up to the second tip vortex, where P and Q mean vorticity and X/D axis, respectively. The reduction of vorticity value relaxed largely after the second tip vortex. In the case of bubble tracers, the reduction rates of vorticity increased highly, and the slope of their fitted equations has the range of from 25.0 to 29.1 up to the second tip vortex. After the second tip vortex the slope of the linear fitted lines had the range of from 5.84 to 7.31. The linear fitted equations regarding the vorticity reduction rate would give some insight into how much vorticity value was underestimated when a PIV technique was employed in the measurements of high velocity gradient flow using bubble tracers.

We found that the differences in tip vortices' vorticity values between solid and bubble tracers are attributed to the large difference in the velocity components around the high velocity gradient region. To investigate the difference in velocity distribution, axial and vertical velocity profiles were extracted at each tip vortex position. The axial velocity

component has smaller magnitude in the bubble tracer cases, especially in the horizontal direction below 0.35 atm. as shown in Fig. 9(b).

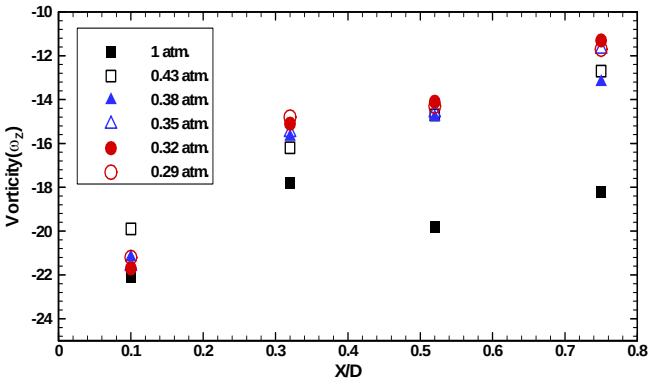

Figure 8: Vorticity distribution at tip vortices according to the variation of tunnel pressure

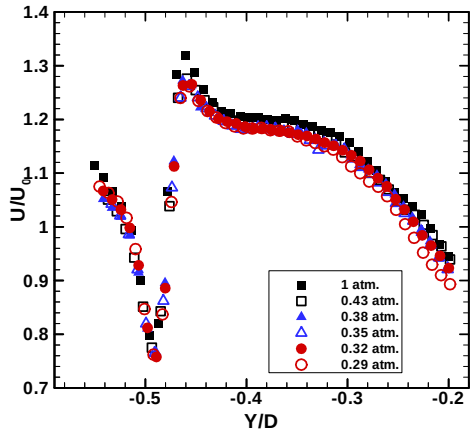

(a) vertical direction

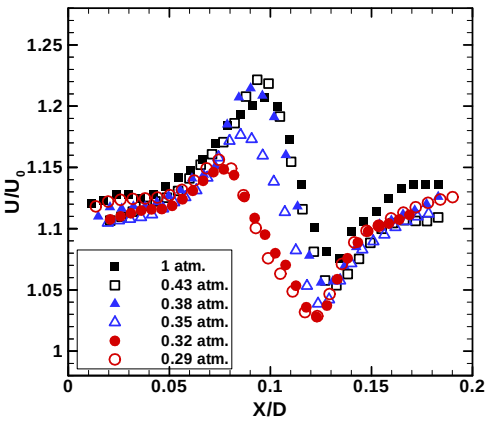

(b) horizontal direction

Figure 9: Axial velocity profiles crossing the first tip vortex in vertical and horizontal directions according to the variation of tunnel pressure

Vertical velocity component also shows some difference but its magnitude is very small because vertical component itself has small values near the tip vortex, comparing to the axial velocity component. Similar tendency appeared in other tip vortices as well. Therefore, the discrepancy in the vorticity value of tip vortices seems to be caused by the difference of the axial velocity between two types of tracers in the horizontal direction.

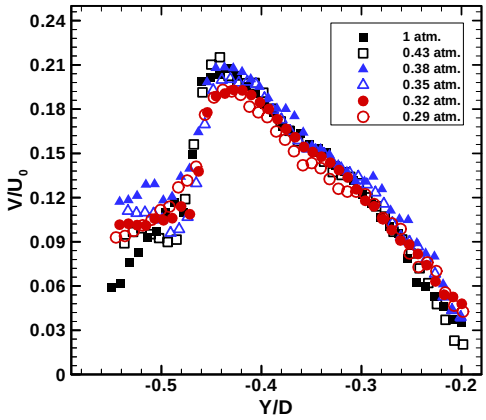

(a) vertical direction

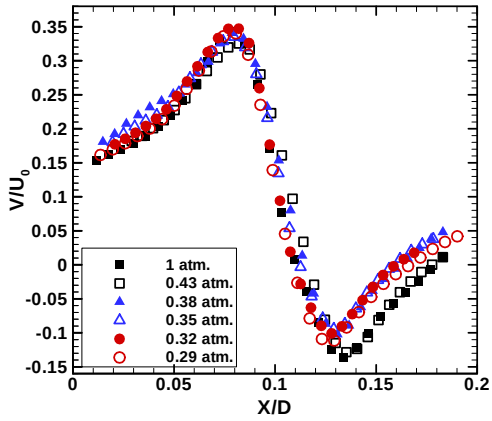

(b) horizontal direction

Figure 10: Vertical velocity profiles crossing the first tip vortex in vertical and horizontal directions according to the variation of tunnel pressure

DISCUSSION

Fitted equations regarding the vorticity reduction would give some reference that is useful for the PIV measurements of high velocity gradient flow using bubble tracers. Normally, tip vortices in a propeller wake have similar vorticity values. At 1 atm. case, they have the range of -22 ~ -18. On the other hand, bubble tracer cases show gradually decreasing vorticity distribution. Bubble tracers show different vortical behavior from solid tracer as the wake moves downstream. Comparing the velocity components around tip vortices, vertical velocity has much different behaviors from axial one as shown in Fig. 11.

The difference in the velocity magnitude between bubble and water is known as slip velocity $U_S = (U_{bubble}-U_{water})/U_0$. U_{bubble} and U_{water} mean the axial velocity magnitude of bubble and solid, and U_0 is the free stream velocity measured by solid

tracers. Figure 12 shows the contours of slip velocity U_S and V_S regarding two propeller wake cases. In the slipstream region of -0.35 <Y/D < -0.10, the velocity difference in the axial direction between solid and bubble was less than 2% of free stream velocity near the trailing vortices, and it has values ranging from 0.15% to 0.5% at the other areas. Although the slip velocity was quite small at the region of small velocity gradient, it might be different in a high velocity gradient region, especially tip vortices. All the tip vortices have U_S larger than 10%, however, their values are similar to each other. In the case of slip velocity V_S in the vertical (radial) direction, the variation of it is different from that of U_S. The first and second tip vortices show small slip velocity, however, other tip vortices exhibit strong slip velocity which is nearly twice the value of the first two tip vortices. This feature directly connected to the vorticity distribution and resulted in vorticity reduction in the downstream wake region.

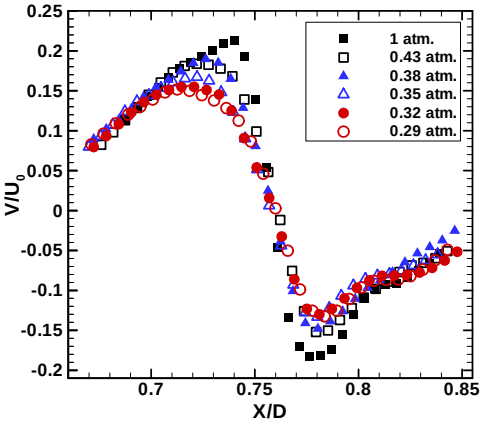

Figure 11: Vertical velocity profiles crossing the fourth tip vortex in horizontal directions according to the variation of tunnel pressure

To investigate the characteristics of a bubbly flow further in a high velocity gradient region, another Reynolds number Re_S was defined by the slip velocity.

$$Re_S = |U_{bubble} - U_{water}|D_{bubble} / \nu$$

Here, D_{bubble} and ν are the mean diameter of the bubbles and the kinematical viscosity of water, respectively. The slipstream region in Fig. 11 gives the range of $15 < Re_S < 75$ when D_{bubble} is supposed to be about 1mm. This Reynolds number range is higher than that ($0 < Re_S < 9$) of the rising bubble case in spite of the similar diameter of bubbles.

The rising bubble gives $1 < C_D$(drag coefficient) < 20. However, it decreased to a range of $0.56 < C_D < 1.85$ when a bubble appeared in a high Reynolds number flow above the transition region, experiencing a small velocity gradient. In the case of the small velocity gradient flow, the drag force on the bubbles was too small to require serious correction of a bubbly flow into a real flow. On the other hand, the high velocity gradient, especially, the tip vortex region (-0.50 < Y/D < -0.35) gives different characteristics of bubbles. The slip velocity became to have the value over 15% at the tip vortex cores. The Re_S was about 1000 because the slip velocity magnitude increased to about $0.2U_0$ at a tip vortex, which can affect the vorticity reduction rate in the vortical structure.

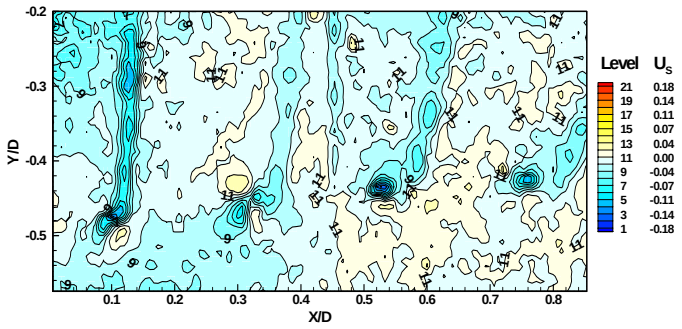

(a) Axial velocity component

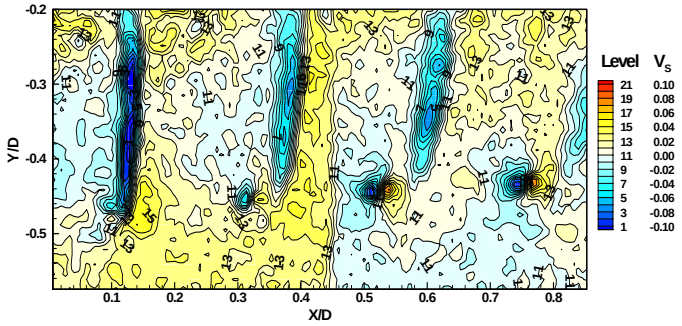

(b) Vertical velocity component

Figure 12: Contour plots of slip velocity at 0.29 atm.

In the next stage, it is necessary to conduct detailed visualizations of vortex core, invaded by entrained bubbles whose size is variable at several Reynolds and cavitation numbers, to figure out the influences of slip velocity.

CONCLUSION

The trace ability of the bubbles was investigated by using a two-frame PIV technique at high Reynolds number over 10^6 in the mid-size cavitation tunnel. The velocity fields in the longitudinal planes were obtained in high velocity gradient flows of the propeller wake.

The bubbles showed rather good trace ability in the high velocity gradient flow. The wake screen arranged in front of a rotating propeller provided a better bubble seeding condition, reducing the interrogation window size more than the case of the uniform flow. The bubbles followed the behaviors of the propeller wake very well in the slipstream region. However, as the flow closes to a tip vortex in a high velocity gradient region, the bubbles showed some discrepancies on the flow behaviors.

A comparison of velocity field data in both tracer cases revealed the reason for the different results. The large slip velocity and Re_S provided a difference especially in the high

velocity gradient region. The slipstream region gives a range of $15 < Re_S < 75$; however, Re_S is about 1000 at a high velocity gradient region of a tip vortex.

The high shear flow seems to influence on the bubbles' deformability and may reduce the Reynolds shear stress. PIV results analyzed by the scattered light images of bubbles might be not enough to explain the bubble's deformability or a slight change in the turbulent flow around it. Additional research is necessary to find out how the bubble tracers affect their deformability and the characteristics of turbulent flow nearby.

ACKNOWLEDGMENTS

This research was supported by the basic research project at MOERI/KORDI(PES128B).

REFERENCES

[1] Paik, B. G., Kim, K. Y., Ahn, J. W., Kim Y. S., Kim, S. P., Park, J. J. 2008, "Experimental study on the Gap Entrance Profile affecting Rudder Gap Cavitation," *Ocean Engineering*, 35, No. 1, 139-149.

[2] Brenn, G., Braeske, H., Durst, F. 2002, "Investigation of the unsteady two-phase flow with small bubbles in a model bubble column using phase-Doppler anemometry," *Engineering Science*, 57, 5143-5159.

[3] Lane, G.L., Schwarz, M.P., Evans, G.M. 2005, "Numerical modeling of gas-liquid flow in stirred tanks," *Chemical Engineering Science*, 60, 2203-2214.

[4] Guet, S., Ooms, G., Oliemans, R.V.A., Mudde, R.F. 2004, "Bubble size effect on low liquid input drift-flux parameters," *Chemical Engineering Science*, 59, 3315-3329.

[5] Lindken, R., Merzkirch, W. 2002, "A novel PIV technique for measurements in multiphase flows and its application to two-phase bubbly flows," *Experiments in Fluids*, 33, 814-825.

[6] Jansen, P.C.M. 1986, "Laboratory observation of the kinematics in the aerated region of breaking waves," *Coast. Eng*, 9, 453-477.

[7] Govender, K., Mocke, G. P., Alport, M. J. 2002, "Video-imaged surf zone wave and roller structures and flow fields," *J. Geophys. Res*., 107, 3072.

[8] Ryu, Yonguk, Chang, Kuang-An, Lim, Ho-Joon 2005, "Use of bubble image velocimetry for measurement of plunging wave impinging on structure and associated greenwater," *Meas. Sci. & Technol*., 16, 1945-1953.

[9] Raffel M, Willert C, Kompenhans J 1998, Particle image velocimetry. *Springer ISBN 3-540-63683-8*.